Biofabrication of Hepatic Constructs by 3D Bioprinting of a Cell-Laden Thermogel

ADVANCED HEALTHCARE MATERIALS
www.advhealthmat.de

Biofabrication of Hepatic Constructs by 3D Bioprinting of a Cell-Laden Thermogel: An Effective Tool to Assess Drug-Induced Hepatotoxic Response

*Manuele Gori, Sara M. Giannitelli, Miranda Torre, Pamela Mozetic, Franca Abbruzzese, Marcella Trombetta, Enrico Traversa, Lorenzo Moroni, and Alberto Rainer**

A thermoresponsive Pluronic/alginate semisynthetic hydrogel is used to bioprint 3D hepatic constructs, with the aim to investigate liver-specific metabolic activity of the 3D constructs compared to traditional 2D adherent cultures. The bioprinting method relies on a bioinert hydrogel and is characterized by high-shape fidelity, mild depositing conditions and easily controllable gelation mechanism. Furthermore, the dissolution of the sacrificial Pluronic templating agent significantly ameliorates the diffusive properties of the printed hydrogel. The present findings demonstrate high viability and liver-specific metabolic activity, as assessed by synthesis of urea, albumin, and expression levels of the detoxifying CYP1A2 enzyme of cells embedded in the 3D hydrogel system. A markedly increased sensitivity to a well-known hepatotoxic drug (acetaminophen) is observed for cells in 3D constructs compared to 2D cultures. Therefore, the 3D model developed herein may represent an in vitro alternative to animal models for investigating drug-induced hepatotoxicity.

1. Introduction

Recent advances in additive manufacturing (AM) techniques have found an application in tissue engineering (TE) to produce free-form porous scaffolds with tailored architectures. AM techniques have dramatically improved the control over scaffold porosity, pore size and interconnectivity, as well as mechanical performance.[1]

Hydrogel biomaterials are compatible with cell encapsulation during the deposition process, opening new avenues in the field of soft tissue engineering. Moreover, direct manufacturing of tissue precursors with a cell density similar to native tissue has the potential to overcome the extensive in vitro culture required by the seeding of prefabricated 3D scaffolds.

Thus, several research groups have adapted different AM techniques to direct the assembly of extracellular matrix (ECM) materials with multiple cell types, and to obtain heterogeneous distribution of drugs and growth factors within controlled 3D architectures.[2,3] Furthermore, viable cell-laden constructs have been successfully fabricated and proposed as in vitro cellular models for pathogenetic and drug discovery studies; the reported applications of cell bioprinting include, among the others, the biofabrication of adipose tissue,[4] bone tissue,[5] liver tissue,[6,7] and cervical tumor models.[8]

Targeting bioprinting applications, hydrogels have to meet specific requirements of viscosity and gelation rate to achieve an accurate match of the designed architecture, therefore limiting the number of formulations that can be processed by bioprinting.[9] Moreover, the gel must be nontoxic, with adequate structural integrity and mechanical properties for in vitro culture and in vivo implantation.[10,11]

Dr. M. Gori, Dr. S. M. Giannitelli, M. Torre, Dr. F. Abbruzzese, Prof. M. Trombetta, Dr. A. Rainer
Department of Engineering
Università Campus Bio-Medico di Roma
via Álvaro del Portillo 21, Rome 00128, Italy
E-mail: a.rainer@unicampus.it

Dr. P. Mozetic
Center for Translational Medicine (CTM)
International Clinical Research Center (ICRC)
St. Anne's University Hospital
Studentská 812/6, Brno 62500, Czechia

Dr. P. Mozetic, Prof. L. Moroni, Dr. A. Rainer
Institute of Nanotechnology (NANOTEC)
National Research Council
via Monteroni, Lecce 73100, Italy

Prof. E. Traversa
School of Energy Science and Engineering
University of Electronic Science and Technology of China
2006 Xiyuan Road, Chengdu, Sichuan 611731, China

Prof. L. Moroni, Dr. A. Rainer
MERLN Institute for Technology Inspired Regenerative Medicine
Department of Complex Tissue Regeneration
Maastricht University
Universiteitssingel 40, Maastricht 6229 ER, the Netherlands

The ORCID identification number(s) for the author(s) of this article can be found under https://doi.org/10.1002/adhm.202001163

DOI: 10.1002/adhm.202001163

When performing crosslinking of cell-laden bioprinted constructs, toxicity issues should be carefully considered. For instance, several common crosslinking agents, such as glutaraldehyde, 1-ethyl-3-(3-dimethylaminopropyl) carbodiimide hydrochloride (EDC), and N-hydroxysuccinimide (NHS), as well as some photoinitiators, have been demonstrated to negatively affect cell viability.[12]

Thus, the combination of different materials arises as a promising route to develop hydrogel matrices with cytocompatible gelation mechanisms and tailored chemomechanical behavior.[13] In this manner, tunable properties can be achieved through the integration of multiple solidification/gelling mechanisms and multistep cross-linking systems.[14,15]

In a previous work, our group demonstrated the successful fabrication of viable constructs with embedded C2C12 myoblasts by direct-write bioprinting of Pluronic/alginate blends.[16] In this method, the direct deposition of a gel is performed, taking advantage of noncovalent bonds that regulate the sol–gel transition of the biomaterial system.[17] Indeed, despite its great potential in extrusion-based bioprinting in terms of printability and shape fidelity, Pluronic has very weak mechanical and structural properties and shows quick degradation as well as rapid dissolution in aqueous solutions.[18] Its combination with a polymer showing a distinct phase transition mechanism has been proven to integrate the advantages of Pluronic thermogel printability, with the enhanced mechanical strength imparted by the temperature-insensitive alginate component. Even though the addition of alginate slightly lowers the sol-gel transition temperature of Pluronic, the latter continues to dictate the thermogel transition behavior, as micelles still undergo temperature-driven rearrangement. Hence, although Pluronic represents the most abundant component of the gel system, unconfined compression tests gave an elastic modulus quite close to the literature data for pure alginate AM scaffolds.[19] Besides, in light of its relatively rapid elution in aqueous solution, the Pluronic component also serves as a sacrificial templating agent with the aim to increase the overall diffusive properties of the hydrogel.

Among the diverse applications of biofabrication, the development of 3D in vitro human hepatic models represents a remarkable alternative to conventional 2D culture systems, also with the potential to overcome the shortcomings related to the use of experimental animals.[20] Although bioprinting of liver tissue has remarkably progressed in the last couple of years, witnessing the generation of functional liver patches from iPSCs-derived hepatic organoids, the use of hepatic cell lines, such as HepG2 cells,[20–23] is still suitable for 3D in vitro assays in a range of applications including toxicology, drug screening, and biology of viral infections.[6,24,25] Bioprinting can introduce additional complexity to these assays for a better representation of liver pathophysiological responses to external stimuli and pharmacological agents.[26,27] Currently, there is a growing interest in harnessing the potential of the bioprinting technology for the development of more advanced and functional in vitro 3D liver models that could be exploited as high-throughput platforms in the drug screening market.[6,28] With the aim to increase the biological relevance of the bioprinted constructs, recent works make use of various instructive cues within the bioinks by the addition of Matrigel, human decellularized extracellular matrix (dECM) and ECM-derived components,[29,30] which demand for a fine tuning in terms of resulting mechanical and viscoelastic properties.[31] Conversely, in this work we chose to develop an in vitro 3D hepatic model using a bioinert Pluronic/alginate composite thermogel, without engineering the 3D microenvironment with cell-instructive signals. We assessed the suitability of such inert biomaterial system in supporting HepG2/C3A hepatoma cell line viability and metabolic activity, in comparison with conventional 2D adherent cultures. Furthermore, given the pivotal role played by liver metabolism in preclinical toxicity studies for the discovery of novel and safe drugs and therapeutic agents,[32,33] we also investigated if our 3D liver platform could represent a valuable and more sensitive tool, compared to adherent controls, for high-throughput screening of hepatotoxic compounds, and for studying the enzymatic biotransformation of nontoxic chemicals to toxic metabolites in vitro.

Collectively, the significance of our hepatic constructs goes far beyond the simple development of a liver model that can mimic the 3D microarchitecture of the hepatic tissue, and addresses some of the challenges and the limitations in the use of non-physiological 2D culture systems for drug discovery purposes, with the long-term goal to reduce animal testing.

2. Experimental Section

2.1. Materials

Sodium alginate powder (Protanal XP 3499) was purchased from FMC BioPolymer (Oslo, Norway); Dulbecco's modified Eagle medium (DMEM), L-glutamine, and penicillin/streptomycin solution were purchased from Lonza (Basel, Switzerland); Pluronic (PF127), FITC-Dextran (MW 20 kDa, FD20S), FITC-labeled phalloidin (P5282), TRITC-labeled phalloidin (P1951), thiazolyl blue tetrazolium bromide (M2128) and acetaminophen (A7085) were purchased from Merck (Darmstadt, Germany); DMEM without phenol red (Gibco), fetal bovine serum (Gibco), BlockAid blocking solution, goat anti-mouse IgG (H+L) Alexa Fluor-488, DAPI (62 248), ProLong Diamond Antifade Mountant (P36961), vybrant cytotoxicity assay (V-23111), ReadyProbes Cell Viability Imaging Kit (Blue/Green), FluoroBrite DMEM (Gibco), Trizol Reagent, high capacity cDNA reverse transcription kit, TaqMan universal Master Mix II and TaqMan Gene Expression Assay primers were purchased from Thermo Fisher Scientific (Waltham, MA, USA); HepG2/C3A cell line (ATCC HB-8065) was purchased from ATCC (Manassas, VA, USA); FITC-conjugated anti-Ki-67 antibody was purchased from Santa Cruz Biotechnology (Dallas, TX, USA); Urea assay kit (ab83362) and human albumin ELISA Kit (ab108788) were purchased from Abcam (Cambridge, UK).

2.2. Bioink Preparation and Characterization

On the basis of the previous findings,[16,34] a blend of 20 wt% Pluronic F127 and 2 wt% sodium alginate was chosen for the fabrication of cell-laden constructs, since this composition was proven as the most suitable for cell encapsulation and printing. The polymeric blend solution was prepared by the so-called "cold method" proposed by Schmolka et al.[35] Briefly, for the preparation of a bioink batch, sodium alginate powder (0.1 g) was slowly

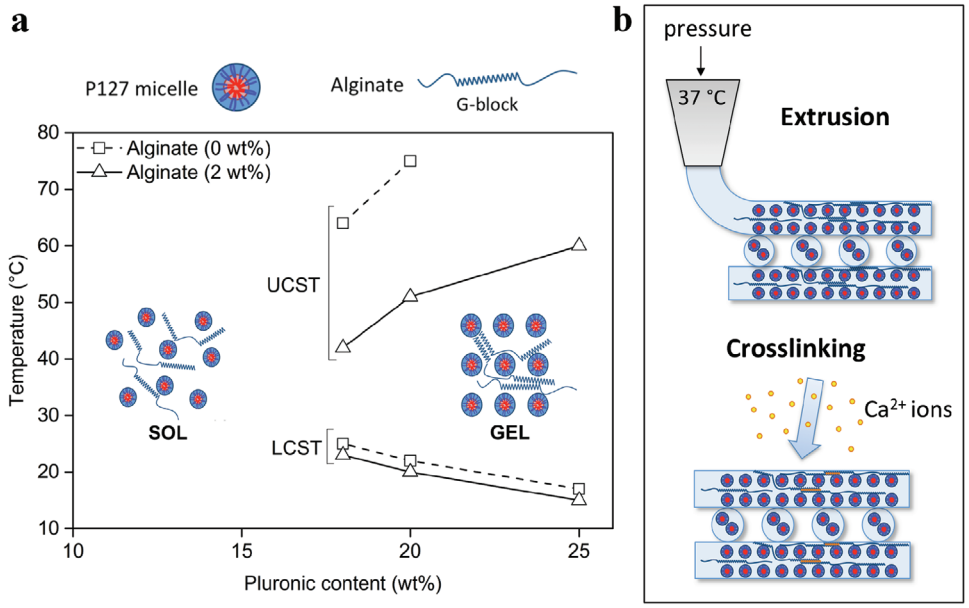

Figure 1. Fabrication of Pluronic/alginate structures. a) Sol–gel–sol transition curves for Pluronic F127/alginate system (UCST, upper critical solution temperature; LCST, lower critical solution temperature). b) Schematic diagram of the direct-write bioprinting process through pressure-assisted extrusion of the hydrogel at 37 °C, followed by chemical crosslinking with Ca^{2+} ions.

added to 3.9 mL of ice-cold DMEM (diluted 1:5 in deionized water) kept under mild stirring for 1 h. Subsequently, Pluronic (PF127, 1 g) was slowly dispersed in the alginate solution under the same conditions. The mixture was stirred until complete dissolution, sterilized by autoclaving and kept at 4 °C until use.

Figure 1 shows the thermosensitive behavior of the Pluronic/alginate system in aqueous solutions (Figure 1a), together with a schematic representation of the crosslinking mechanism after the printing process (Figure 1b).

The thermoresponsive behavior of the Pluronic/alginate solution was more deeply investigated by means of a temperature sweep test (MCR 302, Anton Paar, Austria). After determining the linear viscoelastic region (LVER) with an amplitude sweep test (T = 4 °C, angular frequency ω = 10 s^{-1}, shear strain γ = 0.001%–1%), the temperature sweep test was conducted in the 4–60 °C range with a heating rate of 0.1°C s^{-1} at ω = 10 s^{-1} and γ = 0.01%. The temperature-dependent functions of G' (storage modulus) and G'' (loss modulus) were recorded.

Previous findings demonstrated that the Pluronic component of the gel system is rapidly eluted in aqueous buffer.[34] To investigate whether the loss of the sacrificial templating agent affected the resulting diffusive properties of the gel system, in agreement with data in the literature,[36] a semiquantitative diffusion assay was performed using fluorescence recovery after photobleaching (FRAP). Droplets (≈10 µL) of Pluronic/alginate solution and 2 wt% pure alginate (to be used as a control) were deposited on the surface of a Petri dish and covered with 2.5 × 10^{-2} M calcium chloride solution. Following gelation, specimens were incubated with 0.1 mg mL^{-1} FITC-labeled dextran (MW 20 kDa) in DMEM without phenol red for 48 h.

FRAP experiments were performed on a Nikon A1R+ laser scanning confocal microscope (Nikon, Japan). Gels were placed on a glass coverslip, gently wiped for excess medium and observed under a 20× NA0.7 objective. Photobleaching was performed on a 50 µm circular ROI using a combination of 405 nm (100 mW) and 488 nm (40 mW) lasers. Time lapse images were acquired immediately before and up to 2 min following bleaching using FITC channel and 488 laser line. Measurements of intensity over time in the bleached region were performed using NIS Elements AR software suite (Nikon). Data were compensated for observational photobleaching (using a reference ROI far from the bleached spot) and analyzed in terms of the fluorescence half-time of recovery. Diffusion coefficients were estimated using the model developed by Kang et al.[37]

2.3. Biocompatibility of Nonprinted Bulk Hydrogels

In order to evaluate Pluronic/alginate biocompatibility, cell viability was assessed after encapsulation in bulk hydrogels with volume and cell density comparable to that of bioprinted constructs. A human hepatoma cell line, HepG2/C3A, was chosen for the encapsulation in the hydrogels. Cells were cultured in DMEM supplemented with 10% fetal bovine serum (FBS), 2 × 10^{-3} M L-glutamine, 100 IU mL^{-1} penicillin, and 100 µg mL^{-1} streptomycin (hereinafter, growth medium). After gentle trypsinization, cells were pelleted and homogeneously suspended into ice-cold Pluronic/alginate solution and 2 wt% pure alginate (as a control) at a final concentration of 2 × 10^6 cells mL^{-1}. Droplets of both solutions (50 µL, corresponding to the volume of a bioprinted construct) were dropped into a 2.5 × 10^{-2} M calcium chloride buffer. After gelation, they were retrieved and cultured in growth medium.

Cell metabolic activity was measured using thiazolyl blue tetrazolium bromide (MTT) assay. At each time point (1, 4, and 7 d), activity of mitochondrial dehydrogenases in living cells was measured in terms of absorbance at 570 nm (Tecan Infinite M200-Pro) after 3 h exposure to a 0.5 mg mL^{-1} MTT solution in PBS

at 37 °C, 5% CO_2. Absorbance values obtained in the absence of cells were used for background subtraction.

Cell viability was further investigated by fluorescence imaging using the ReadyProbes Cell Viability Imaging Kit (Blue/Green). Briefly, nonprinted bulk hydrogels were both rinsed in saline solution and incubated with the Imaging Kit for 30 min at 37 °C in complete FluoroBrite DMEM. The NucBlue Live reagent stains the nuclei of all cells, whereas the NucGreen Dead reagent selectively detects only the nuclei of dead cells with compromised plasma membranes. Micrographs were acquired using a Nikon A1R+ laser scanning confocal microscope (Nikon, Japan).

2.4. Additive Manufacturing

Direct-write deposition of the Pluronic/alginate gel was performed using a custom-designed equipment,[38,39] consisting of an X–Y motorized stage (model PLS-85, PI miCos GmbH, Germany) for the positioning of the dispensing head, and a z-axis (LS-85, PI miCos) to control its distance from the stage. Generation of the process tool-path was performed starting from a computer-aided design input geometry using a dedicated software interface. The printing head consisted of a 5 mL pneumatic dispensing syringe (Nordson, OH) equipped with a heating jacket and a 250 µm ID blunt end dispensing tip.

As previously described,[34] the Pluronic/alginate mix was loaded into the syringe in sol state, connected to a pressure controller (OB1, 4 channel microfluidic flow controller, Elveflow, Paris, France), and kept at 37 °C until gelation. The mixture was then extruded into a sterile slide through a 250 µm orifice at a pressure of 0.8 bar with a relative speed between the nozzle and the X–Y table of 1.3 mm s^{-1}. Squared structures (10 mm side) with a homogeneous fiber spacing (1 mm) were obtained by depositing four layers of fibers in a wood-pile structure. After bioprinting, the structures were briefly exposed to a 2.5×10^{-2} M $CaCl_2$ aqueous solution to induce alginate crosslinking. After 5 min, the crosslinked constructs were transferred to cell culture medium, with frequent medium changes in the first hours to ease the dissolution of the Pluronic component.

2.5. Fabrication of Cell-Laden Constructs

Bioprinting of cell-laden constructs (hereinafter, GEL) was performed as described above. HepG2/C3A cells were trypsinized, pelleted and homogeneously suspended into ice-cold sterile Pluronic/alginate solution at a final concentration of 2×10^6 cells mL^{-1}. The same number of cells was used for 2D adhesion controls (hereinafter, ADH) on 12-well TC-treated multiwell plates (Falcon, BD Biosciences, NJ), corresponding to a density of 1.1×10^4 cells cm^{-2}. Both GEL and ADH groups were cultured in growth medium. Fresh medium was renewed daily and supernatants collected for analysis of cell metabolites.

2.6. Fluorescence Microscopy

Staining solutions for the processing of GEL constructs were prepared in a saline solution buffer (0.9% w/v aq. NaCl) containing 2.5×10^{-2} M $CaCl_2$. After washing, GEL constructs were fixed in 4% paraformaldehyde (PFA) for 15 min. After fixation, samples were washed in 1×10^{-3} M glycine in saline solution, and subsequently permeabilized with 0.1% Triton X-100 for 10 min. F-Actin was revealed with FITC-labeled phalloidin (1:400 for 45 min).

For indirect immunostainings, scaffolds were first blocked in BlockAid blocking solution for 45 min at room temperature (RT) and then incubated with FITC-conjugated anti-Ki-67 antibody (mouse monoclonal IgG1) diluted 1:400 in BlockAid blocking solution overnight at 4 °C. After careful washing with saline solution, goat anti-mouse IgG (H+L) Alexa Fluor-488 secondary antibody was incubated for 1 h at RT in the dark in blocking solution. F-Actin was revealed with TRITC-labeled phalloidin (1:400 for 45 min) and nuclei were counterstained with DAPI (1:10 000 for 10 min). Samples were washed and mounted on glass-bottom Petri dishes (CellView, Greiner Bio One, Austria) with ProLong Diamond Antifade Mountant. Micrographs of GEL constructs were captured using a Nikon A1R+ laser scanning confocal microscope.

Micrographs were analyzed in terms of cluster size and percentage of Ki-67-positive cells using the NIS Elements AR software.

2.7. Analysis of Cell Viability and Metabolic Activity of 3D Printed Constructs

Cell viability was assessed using vybrant cytotoxicity assay as previously described.[40] Briefly, the release of the cytosolic enzyme glucose 6-phosphate dehydrogenase (G6PD) from damaged cells into the surrounding medium was quantified after 24 h. 50 µL of supernatant from each specimen was transferred into a 96-well plate and, after 10 min incubation with 50 µL of resazurin/reaction mixture at 37 °C in 5% CO_2, the fluorescent metabolite of resazurin (resorufin) was detected (ex. 530 nm; em. 570 nm) on a Tecan Infinite M200-Pro multiplate reader (Tecan, Switzerland).

Cell metabolic activity was assessed by means of the MTT assay as previously described for bulk nonprinted hydrogels at the same time points (i.e., 1, 4, and 7 d). Each experiment was performed in triplicate.

2.8. Urea and Albumin Secretion Assays

The levels of urea and albumin secreted by HepG2 cells during the culture period (at 1, 4, and 7 d) were determined on culture supernatants using a colorimetric test (Urea Assay Kit) and an ELISA kit (Human Albumin ELISA Kit), respectively, according to the manufacturer's instructions. Readings were performed using a microplate reader (Tecan Infinite M200-Pro), and metabolite levels were quantified against the kit standard curves and expressed as µg per day per million cells.[41–43] Cells were counted through the Trypan blue exclusion method using the TC20 Automated Cell Counter (Bio-Rad Laboratories, CA, USA). Experiments were performed in triplicate.

2.9. Hepatotoxicity Assay

Hepatotoxicity testing was performed using acetaminophen (paracetamol, APAP) as a model drug.

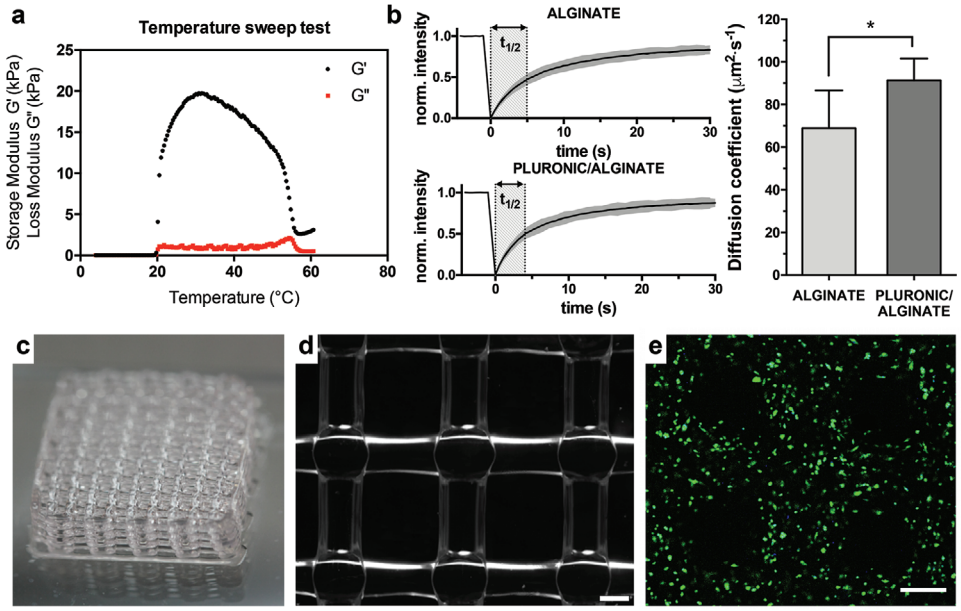

Figure 2. a) Rheological characterization of Pluronic/alginate ink: storage and loss moduli as function of temperature. b) FRAP analysis: mean (black line) and 95% confidence interval (solid gray band) of FRAP curves for Pluronic/alginate and pure alginate gels. Bar plot of the diffusion coefficient of 20 kDa FITC-dextran in the two hydrogels as estimated from the FRAP curves ($p = 0.023$). c–e) Microscopic characterization of bioprinted constructs: c) macrograph (1 cm ×1 cm × 0.25 cm), d) optical micrograph of a multilayered hydrogel structure (scale bar: 250 μm) and e) confocal micrograph of HepG2 cells in hydrogel constructs at day 0 (scale bar: 200 μm). Actin cytoskeleton was labeled with FITC-phalloidin (in green).

To identify the subtoxic concentration range of the drug, a dose–response curve was established. From a stock solution of acetaminophen 0.5 M in EtOH, seven consecutive dilutions in complete medium were prepared within a range from 0 to 8×10^{-2} M. Each dilution was prepared in triplicate. Cell viability was assessed after 24 h exposure by means of the MTT assay as described above. The dose–response curve was obtained as a semilogarithmic plot by using a Variable Slope fitting model (GraphPad Prism ver 6.0, GraphPad Software, CA, USA). A subtoxic dose of 1.4×10^{-2} M was chosen for the assay. Internal controls were represented by administration of corresponding volumes of culture medium without APAP.

Drug administration was commenced 7 d after printing and fresh drug-containing medium was renewed daily. Cell viability was evaluated at 24 and 48 h after drug administration through the MTT assay. Experiments were performed in triplicate and data were normalized against their internal controls.

2.10. CYP1A2 Expression Levels

Expression of CYP1A2, a member of cytochrome P450 superfamily involved in the metabolism of xenobiotics, was evaluated by means of quantitative reverse transcription polymerase chain reaction (qRT-PCR) on both ADH and GEL groups. Isolation of mRNA was performed using TRIzol reagent. Extracted RNA was quantified spectrophotometrically (NanoQuant plate on Tecan Infinite M200-Pro). 1 μg of total RNA was retrotranscribed using high capacity cDNA reverse transcription kit according to the manufacturer's instructions. qPCR was performed on 20 ng of cDNA in a total reaction volume of 10 μL on an ABI 7900HT fast real-time PCR System (Thermo Fisher Scientific) using TaqMan universal Master Mix II and TaqMan Gene Expression Assay primer for CYP1A2 (Hs00167927_m1). Analysis of expression levels of a panel of reference genes was performed through geNorm v.3.5.,[44] and beta-2-microglobulin (B2M, Hs00187842_m1) was selected as an endogenous control.

2.11. Statistical Analysis

Data are presented as mean ± standard deviation (SD) of at least three independent experiments. Statistical analysis was performed using GraphPad Prism ver. 6.0. One-way or two-way ANOVA (followed by Tukey post hoc test) were used as appropriate for multiple group comparisons. Significance was at the 0.05 level.

3. Results

3.1. Bioink Characterization

The bioink storage and loss moduli as a function of temperature during the sol-gel transition are reported in **Figure 2**a. Curves were obtained at a constant shear strain in the LVER ($\gamma = 0.1\%$), as determined from a preliminary amplitude sweep test. Sol-to-gel transition occurs at 19 °C, resulting in a rapid increase of G' values. After gel formation ($G' > G''$), the storage modulus approaches a steady value (18.4 kPa). For increasing temperatures, the solution turns back into the sol-state and the storage modulus starts to decrease.

Steady state phase of the solution enables the printing of a stable gel at physiological temperature (37 °C) and mild extrusion pressure (less than 1 bar).

A statistically significant increase (≈32%, $p < 0.05$) in the diffusion coefficient of 20 kDa FITC-dextran was reported for Pluronic/alginate system compared to pure alginate (Figure 2b), indicating that the elution of the sacrificial Pluronic component reflected into augmented diffusive properties of the gel.

3.2. Preliminary Investigation of Nonprinted 3D Controls

Prior to testing cell viability and metabolic activity of the 3D GEL group, we preliminarily investigated cell behavior in bulk pure alginate and Pluronic/alginate hydrogels (with the same composition of the printed bioink) as 3D controls (Figure S1, Supporting Information). Thus, we first performed an MTT assay to compare cell metabolic activity between the two bulk hydrogels throughout one week in culture at three different time points: 1, 4, and 7 d (Figure S1a, Supporting Information). Pluronic/alginate outperformed pure alginate at each time point, with statistically significant differences at day 4 ($p < 0.001$) and day 7 ($p < 0.01$). We also carried out a two-color nuclear staining assay (NucBlue/NucGreen) for evaluating and comparing cell viability of the two bulk 3D controls at day 7 by fluorescence imaging (Figure S1b,c, Supporting Information). The analysis of confocal images for both constructs clearly showed an increasing rate of cell death towards the hydrogel core, thus not representing proper controls for our 3D in vitro model. As a matter of fact, none of the hydrogels was found to be suitable for the fabrication of bulk 3D controls with the same volume of bioprinted constructs, due to the very low level of cell viability observed in the core of the hydrogels, approximately a few hundred microns below the surface. For this reason, cell metabolism and drug response have been studied adopting a "3D bioprinted versus 2D adhesion" experimental design. At the same time, however, the pure alginate hydrogel has been introduced as a control for the determination of the increased diffusive properties of the Pluronic/alginate system by FRAP.

3.3. Biocompatibility Characterization of Pluronic/alginate Scaffolds

Figure 2c,d shows representative macrographs and optical micrographs of the multi-layered constructs, respectively. Both the uniformity of the porous texture and the high-shape fidelity demonstrated the suitability of the described bioprinting technique to precisely lay down fibers directly in the gel state. Indeed, as already shown in a previous work,[34] a very close match between the computer-generated geometry and the obtained construct was achieved (Figure 2d), (mean fiber diameter: 303 ± 5 µm; Image J, National Institutes of Health, USA).

To rule out potential downsides of the printing process, a preliminary characterization was performed by comparing pre- and post-printing cell viability levels (Figure S2 in the Supporting Information).

To analyze the HepG2 spatial organization in a 3D microenvironment, we performed fluorescence staining of actin cytoskeleton in the GEL group at day 0 (soon after printing). The confocal micrograph reported in Figure 2e showed a homogeneous distribution of cells, with morphological characteristics similar to conventional 2D cultures, arranged in a wood-pile pattern according to the construct architecture.

Postprinting viability of the GEL group, measured by G6PD assay on culture supernatants, showed a cell viability close to 95%, after 24 h in culture (**Figure 3**a), in agreement with the average values reported in the literature.[5,8] The difference with ADH controls, although significant, was minimal (94.4 ± 0.5% in GEL vs 98.8 ± 0.2% in ADH), suggesting a very good biocompatibility of both the extrusion process and the biomaterial itself. The analysis of cell metabolic activity, performed by the MTT assay, which can be to some extent correlated to cell proliferation,[41,45] was performed throughout one week in culture at the three time points mentioned above, i.e., 1, 4, and 7 d. Results of the MTT assay (reported as OD values in Figure 3b) did not reveal any statistically significant difference between GEL and ADH groups at all time points. Furthermore, immunofluorescence staining against Ki-67, a nuclear marker for cell proliferation, showed the formation of large-size and compact 3D clusters of cells at day 7 in the GEL group (Figure 3c,d), with a remarkable percentage of Ki-67 positive nuclei (63.6 ± 7.1%), which were also present in the inner core of the cell clusters. This result concurs with the above reported MTT assay, thus confirming an increasing cell proliferation activity in the GEL, as also shown by the statistically significant increase of the 3D clusters size from day 1 to day 7 (Figure 3e). Altogether, these results indicate that the Pluronic/alginate hydrogel is permissive for high survival and proliferation of hepatic cells, with no reported formation of necrotic cores in the clusters. Figure S3 (Supporting Information) shows confocal micrographs demonstrating the homogeneous presence of HepG2 clusters along the fibers at day 7 (25 ± 1.8 clusters above 30 µm in size per mm of hydrogel fiber) with overall good cell viability.

3.4. Analysis of Liver-Specific Metabolic Activity

Besides cell viability and proliferation assays, a more detailed characterization of specific liver activity in terms of hepatic cell metabolism was carried out.

Figure 4 shows the results of urea (Figure 4a) and albumin (Figure 4b) secretion assays, both of which indicated significant differences between GEL and ADH groups. Overall, there was a main effect of culture time ($p < 0.0001$) and culture conditions (GEL vs ADH, $p < 0.0001$) on urea synthesis, as well as an interaction between the two independent variables ($p < 0.0001$). The increase in urea production from day 1 to day 7 was more pronounced for hydrogel-embedded cells than for 2D controls. Post hoc testing revealed a statistically significant increase at day 4 (1.5-fold, GEL vs ADH) and day 7 (3.3-fold, GEL vs ADH). A similar trend was observed for albumin production (Figure 4b). Overall, main effects of culture time ($p < 0.0001$) and culture conditions ($p = 0.013$) were reported: however, each main effect differed across levels of the second independent variable ($p < 0.0001$). GEL group showed an increase in albumin secretion with increasing the culture time, while ADH controls showed almost constant secretion levels. Excluding day 1, the synthetic

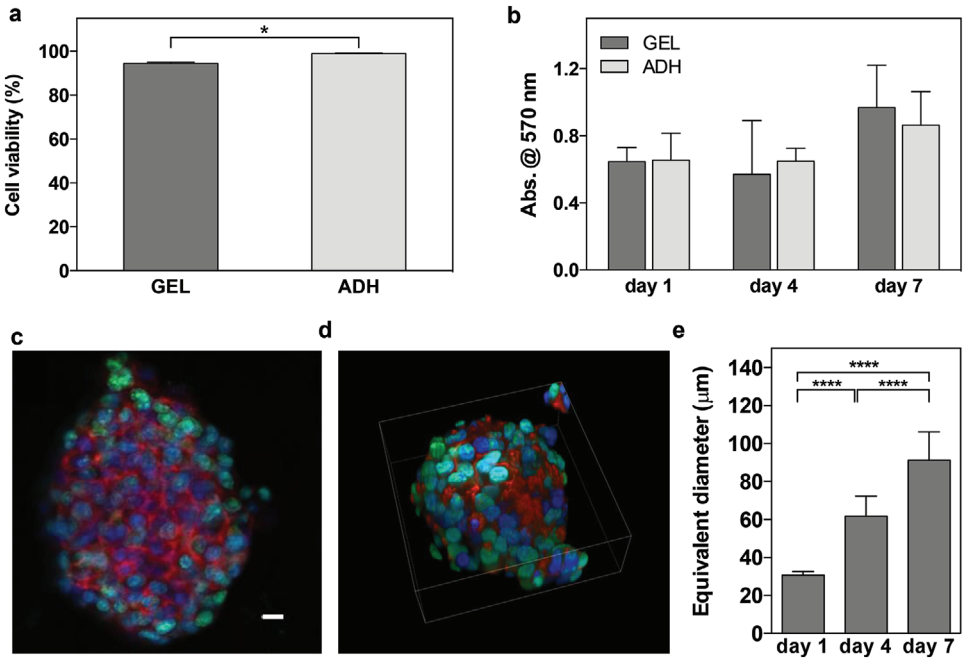

Figure 3. HepG2 cell viability and proliferation. a) Cell viability and b) metabolic activity assays performed on GEL and ADH groups by G6PD and MTT assay, respectively. Fully lysed controls were used to express cell viability as a percentage (%) in (a). c) Immunofluorescence staining against the nuclear antigen Ki-67 (FITC, in green) of large and frequent cell clusters in the GEL at day 7; actin cytoskeleton was labeled with TRITC-phalloidin (in red), and nuclei were counterstained with DAPI (in blue). d) Representative 3D rendering of confocal Z-stack immunofluorescence image against Ki-67 of a cell cluster. Scale bar: (c) 10 μm. e) Equivalent diameter (μm) of cell clusters in bioprinted constructs at each time point. Results are the mean ± SD of at least three independent experiments. * $p < 0.05$, **** $p < 0.0001$.

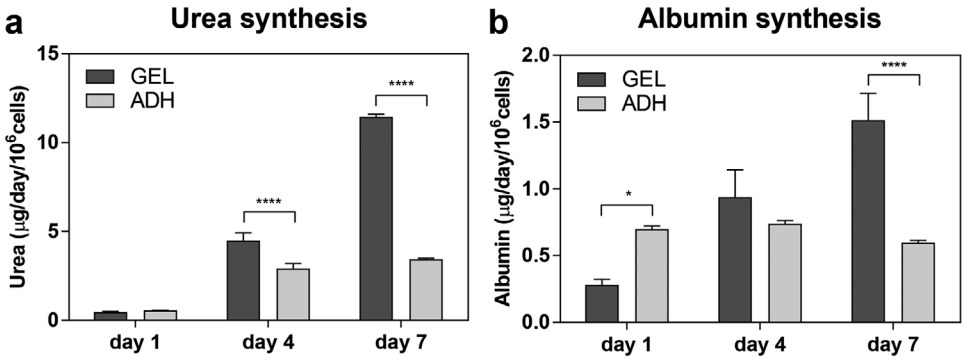

Figure 4. Analysis of liver-specific metabolic activity of HepG2 cells. a) Urea and b) albumin secretion assays after 1, 4, and 7 d in GEL and ADH groups. Metabolite levels were expressed as μg per day per million cells. Results are the mean ± SD of at least three independent experiments. Statistically significant differences between GEL and ADH groups within each time point are indicated as follows: * $p < 0.05$, ** $p < 0.01$, *** $p < 0.001$, **** $p < 0.0001$.

activity of HepG2 in the GEL group outperformed that of ADH controls at day 4 and day 7 (1.3- and 2.5-fold increase, respectively), the latter time point showing high significance ($p < 0.0001$). Overall, HepG2 cells within the hydrogel remained viable and functional, as demonstrated by G6PD and MTT assays, and performed better than 2D control cells in terms of metabolic activity, as shown by the levels of urea and albumin secretion throughout the 1 week culture period. Altogether, these results prompted us to choose day 7 as the optimal condition to test the response of the 3D GEL to a known hepatotoxic drug and compare it to the 2D ADH control.

3.5. Hepatotoxicity Testing of 3D GEL versus 2D Adhesion Control

To explore the potential of the 3D construct as an in vitro platform for toxicological studies, we set out to investigate its response to APAP. In order to select the ideal sublethal drug concentration for the hepatotoxicity test, we first performed a preliminary dose-response curve on HepG2 cells cultured in adhesion using the MTT assay (**Figure 5**a). We found the value 1.4×10^{-2} M as the ideal sublethal APAP concentration corresponding to the LC_{25} level (i.e., the concentration at which the drug produces 25%

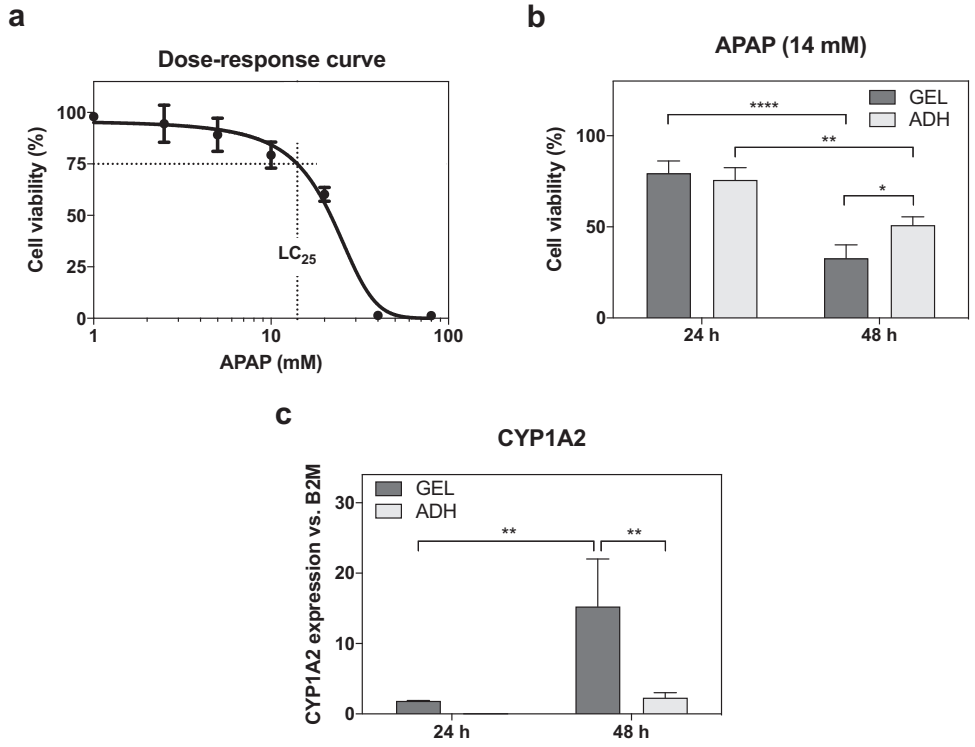

Figure 5. APAP-induced hepatotoxicity on HepG2 cells. a) Dose–response curve of APAP using the MTT assay showed an LC_{25} of 1.4×10^{-2} M. The solid line represents the fitted curve according to variable slope model of GraphPad Prism. b) APAP-induced cytotoxicity in GEL and ADH groups, after 24 and 48 h, expressed as % change of cell viability normalized against their internal controls, measured through the MTT assay. c) Expression of cytochrome CYP1A2 in GEL and ADH groups, as measured 24 and 48 h following APAP administration. Results are the mean ± SD of at least three independent experiments. Statistically significant differences are indicated as follows: * $p < 0.05$, ** $p < 0.01$, *** $p < 0.001$, **** $p < 0.0001$.

lethal effect on cell viability), consistently with other reports.[46–48] Thus, we used this concentration for the administration of APAP to both GEL and ADH groups for 24 and 48 h after the 7 d culture period (Figure 5b). The time points used were chosen according to the literature.[24,32,49,50] Interestingly, in our experiments, HepG2 cells showed different cytotoxic response to APAP (at 1.4×10^{-2} M concentration) when cultured in the GEL system compared to the ADH groups after 24 and 48 h exposure. Overall, HepG2 viability was affected by exposure time ($p < 0.0001$), but this main effect was qualified by an interaction with culture conditions (ADH vs GEL, $p = 0.0185$). Specifically, cell viability at 48 h in the GEL group was significantly lower than in the ADH group (cell survival: 32.7 ± 7.4% vs 52.0 ± 5.9%, $p < 0.05$). This result is apparently attributable to the 3D microenvironment that represents a more physiologically relevant system compared to 2D cultures, as also supported by the literature.[32,50–53] Therefore, we decided to investigate the possible involvement of differential detoxification enzyme activity between GEL and ADH groups. HepG2 cells represent a well-established and reliable model for evaluating the cytochrome P450 (CYP450) enzyme activity in drug metabolism, comparable, to some extent, to human hepatocytes.[54] This enzyme family is particularly expressed in the liver and presents the highest number of CYP isoforms.[55] In particular, CYP1A2 is one of the main isoforms that catalyzes phase I reactions in human drug metabolism.[52] It represents about 13% of CYP enzymes in the human liver, and is involved, among others, in APAP metabolism.[56–58]

However, in traditional 2D cell cultures, HepG2 cells express low levels of CYP450 enzymes.[59] On this basis, we decided to assess basal gene expression levels of CYP1A2 in both GEL and ADH groups at the two time points used for the MTT assay (i.e., 24 h and 48 h following drug administration). We reported main effects of exposure time (24 h vs 48 h, $p = 0.0039$) and culture conditions (ADH vs GEL, $p = 0.0054$) on the upregulation of CYP1A2 mRNA levels, as well as significant interaction between the two independent variables ($p = 0.0216$). Notably, the difference between 2D and 3D cultures became statistically highly significant only after 48 h ($p < 0.01$) Furthermore, the expression of CYP1A2 in the GEL group was significantly upregulated between 24 and 48 h ($p < 0.05$).

This upregulation of CYP1A2 is indeed in agreement with similar data in the literature for both hepatocytes[49] and HepG2 cells[47] in a 3D setting, with the latter work showing how 3D HepG2 spheroids present higher mRNA levels of CYP1A2 versus 2D cultures, although the increase becomes remarkable between 7 and 14 d in their experimental conditions.

4. Discussion

An ideal gel for the biofabrication of cell-laden constructs should be a free-flowing liquid with low viscosity under nonphysiological conditions, and it should undergo a rapid phase transition to form a stable gel capable of withstanding shear forces under physiological conditions.[9,12] Poly(ethylene

oxide)–poly(propylene oxide)–poly(ethylene oxide) triblock copolymers—also known as Poloxamers or by the trade name Pluronic—constitute a group of important thermo-responsive materials, which are capable of producing low viscosity aqueous solutions at ambient temperature and forming a gel at higher temperatures (reverse thermal gelation).

In this work, 3D constructs were bioprinted with controlled architectures and high-shape fidelity and manufactured starting from a composite bioinert Pluronic/alginate thermogel. This polymer blend represents a likely candidate for additive manufacturing since Pluronic confers thermosensitive features, while alginate component gives a strong gel upon exposure to bivalent cations in aqueous solution. The system was exploited to fabricate a novel 3D liver platform for modeling liver metabolism and hepatotoxicity in a more realistic fashion than 2D hepatic cell cultures.

Cultured cells are dramatically affected by the surrounding microenvironment that may influence their growth properties, specific functions, and gene expression, and this aspect is particularly evident when 3D culture systems are compared to conventional 2D cultures.[60,61] Results from recent studies have shown that in vitro performance of hepatic cells is improved when cultured on prefabricated 3D scaffolds[41] or in a 3D environment,[62] such as in spheroids.[24] Although representing the gold standard in liver-like culture systems, hepatic spheroids are still limited by poor nutrient and oxygen supply to the cells of the innermost compartment, hence reducing cellular metabolism and impairing the diffusion rate of nutrients to the cells.[63] In this regard, the peculiar feature of the Pluronic component to be easily removed by elution leads to a specific porous structure,[20,36] which may facilitate diffusion of nutrients and metabolites within the remaining 3D alginate matrix. This couples with the high resolution offered by the direct-write process, which allows the deposition of orderly layered and non-collapsed fibers with a diameter of ≈250 µm (this value is reported in the literature as the limit for viable hepatic constructs without a necrotic core[50,64,65]), further augmenting the exchange of nutrients and metabolic waste products with the culture medium.

The results presented herein demonstrate that our thermogel-based bioprinting technique is effective in prototyping regularly shaped cell-laden constructs, and that such a 3D environment can influence liver-specific functions of HepG2 cells. Furthermore, our 3D engineered liver model is capable of sustaining not only hepatic cell survival and proliferation, but also liver-specific metabolic activities, such as albumin and urea production, as well as sensitivity to hepatotoxic compounds, showing potential application as a 3D in vitro platform for drug-induced hepatotoxicity and toxicological studies. Indeed, APAP has been selected as a candidate drug to assess this potential in vitro. APAP is a common analgesic and antipyretic drug that is safe at therapeutic levels, but it represents the main cause of acute liver failure in the US and the UK, being able to cause liver injury at high doses.[66] This drug is toxic to cells after metabolism in the liver, owing to the formation of reactive hepatotoxic intermediates, such as N-acetyl-p-quinoneimine, generated through oxidation by cytochrome P450 enzymes, which lead to mitochondrial injury, formation of protein adducts and oxidative stress, and in turn to a depletion in cellular glutathione levels required for hepatotoxic intermediate detoxification. The final outcome of this metabolic route is a significant decrease in cell viability via different molecular mechanisms investigated by others.[67,68]

The increased sensitivity to APAP (Figure 5b) and the augmented gene expression of the CYP1A2 enzyme (Figure 5c) from 24 to 48 h, compared to the ADH control, clearly testify the enhanced drug testing performance of our constructs, way better than traditional 2D culture systems. Hepatic models that use traditional 2D mono- and cocultures of normal and diseased human cells fail to mimic the complex 3D in vivo microenvironment and extracellular matrix scaffolding, thereby such models cannot mimic normal cellular functions and physiological responses to the tested drugs.[69–71] In addition, it is widely acknowledged that standard culture plasticware for 2D adherent cultures poorly recapitulates the native tissue microenvironment, whereas more advanced biomaterials, and most of all biocompatible hydrogels, as the one herein presented, can overcome the mechanical and structural limitations of the former, thus positively influencing cell survival and metabolism, as brilliantly reviewed by Caliari and Burdick.[72] Accordingly, our 3D hydrogel can fill this gap, and it represents a more reliable culture system to address some of the challenges of in vitro drug screening, with the aim to obtain a drug response of higher pathophysiological relevance. This advantage, coupled to the opportunity to precisely control the 3D microarchitecture and the specific gel chemistry and texture, is key to reproducing a tissue-like scenario. Thanks to its cellular biocompatibility without the addition of human bioactive components, this 3D approach produces a suitable microenvironment for investigating liver metabolism, which better approximates an in vivo pathophysiological setting, paving the way for further liver studies using also additional types of hepatic cells. Indeed, to better mimic cell–cell and cell–ECM interactions present in the native liver, and to increase the complexity of the tissue microarchitecture, in future works we plan to fabricate 3D hepatic constructs composed by different hepatic cell populations, including parenchymal (primary hepatocytes or hepatoma-derived cell lines) and nonparenchymal cells (such as endothelial, Kupffer, and hepatic stellate cells), which will be proportioned in appropriate physiological ratios according to previously reported studies.[52,73]

In other works, functionalization with ECM components or RGD-motifs was used to create a microenvironment that drives and directs the spatial arrangement of hepatic cells via biological cues, thereby increasing cell metabolism and biosynthetic activities.[74,75] Our strategy of using a bioinert 3D hydrogel leaves hepatic cells free to acquire a 3D spatial conformation (as confirmed by the reported formation of 3D spheroids in the hydrogel matrix), without the need for instructive signals from the surrounding scaffold. Such 3D spheroid generation is most likely due to the intense proliferative activity, proved by the Ki-67 positive expression, not excluding the contribution of cell aggregation within the fibers.

Although primary human hepatocytes are the preferred model for in vitro studies on hepatic metabolism, the HepG2/C3A cell line used herein retains many characteristics of normally differentiated and quiescent hepatocytes, expressing a wide variety of liver-specific metabolic functions, such as components of cholesterol and triglyceride metabolism, among others.[76,77] Thus, the combination of HepG2 cells with our thermogel-based

bioprinting technique turned out to be an improved and easily manageable hepatic cell culture system, suitable to maintain the biological functions of hepatic cells in vitro and to control their metabolic behavior.

Additionally, our results support the hypothesis that the specific 3D arrangement is responsible for the reported upregulation of the CYP1A2 enzyme, which is centrally involved in detoxification pathways.

In this regard, we acknowledge that further studies will be necessary for a thorough validation of the proposed model, which may include the characterization of additional components of the P450 superfamily, as well as the measurement of the expression of other markers of hepatic metabolism, such as albumin, transferrin, beta-lipoprotein, 3-hydroxy-3-methylglutaryl-CoA reductase, hepatic triglyceride lipase, catalase, etc., at both mRNA and protein level, so as to achieve a better understanding and a more exhaustive overview of the various hepatic cell metabolic activities in such a 3D environment.

Although our system represents a proof-of-principle model of a 3D hepatic construct for drug toxicity tests, our results support the hypothesis that hepatotoxicity analysis using 3D culture models may be more likely to reflect true physiological responses to cytotoxic compounds than existing 2D culture systems.[25,61,78] Indeed, the loss of liver-specific metabolic functions in HepG2 cells cultured in 2D can cause reduced biotransformation of potentially toxic compounds, leading to a false evaluation of their potential toxicity. Based on this assumption, our novel 3D liver construct, created by bioprinting of a Pluronic/alginate thermogel, may represent a promising alternative platform for toxicological studies of hepatic metabolism, and potentially for testing new drugs in a more in vivo-like liver microenvironment. In fact, despite almost equal conditions of cell survival and proliferation compared to conventional 2D cultures, our hydrogel system showed increased liver-specific metabolic activities in such a more complex 3D microarchitecture. Accordingly, the results obtained in the GEL group following APAP administration suggest that the increased sensitivity of HepG2 cells to APAP compared to the ADH group is likely due to their culture conditions in a 3D arrangement, as also recently pointed out by other groups.[24,53] As a matter of fact, this 3D microenvironment preserves a cell behavior much closer to the in vivo setting than traditional 2D cultures. This may place the cells under increased oxidative stress, thus inducing the higher levels of cytotoxicity detected in our experiments.

5. Conclusion

In this work, a thermogel-based bioprinting process was successfully adopted for the fabrication of a 3D hepatic cell-laden hydrogel. Here, we developed a 3D in vitro bioprinted model, without the addition of instructive signals, which is characterized by clusters of hepatic cells into a hydrogel with ameliorated diffusive properties. The present model demonstrates higher cell metabolic performance compared to traditional 2D cultures. This increased metabolic competence may find an application in toxicological studies, such as for the reported model drug, representing a candidate in vitro alternative method to predict in vivo drug hepatotoxicity.

Supporting Information

Supporting Information is available from the Wiley Online Library or from the author.

Acknowledgements

M.G. and S.M.G. contributed equally to this work. This work was partially supported by MIUR-FIRB program (grant no. RBFR10L0GK). M.G. was supported by a Fellowship from FIRE "Fondazione Italiana per la Ricerca in Epatologia" Onlus (FIRE Fellowship 2017). P.M. acknowledges support from the European Social Fund and the European Regional Development Fund (CZ.02.1.01/0.0/0.0/15_003/0000492 "Unveiling the molecular determinants of aging to design new therapeutics - MAGNET"). P.M., L.M. and A.R. are thankful to "Tecnopolo per la medicina di precisione" (TecnoMed Puglia) - Regione Puglia: DGR n.2117 dated 21/11/2018, CUP: B84I18000540002 and "Tecnopolo di Nanotecnologia e Fotonica per la Medicina di Precisione" (TECNOMED) - FISR/MIUR-CNR: delibera CIPE n.3449 dated 07/08/2017, CUP: B83B17000010001.

Conflict of Interest

The authors declare no conflict of interest.

Keywords

3D liver models, bioprinting, drug hepatotoxicity, hepatic constructs, Pluronic/alginate thermogels

Received: July 6, 2020
Revised: August 23, 2020
Published online: September 17, 2020

[1] S. M. Giannitelli, A. Rainer, D. Accoto, S. De Porcellinis, E. M. De-Juan-Pardo, E. Guglielmelli, M. Trombetta, in *Tissue Engineering: Computer Modeling, Biofabrication and Cell Behavior*, (Eds: P. R. Fernandes, P Bartolo), Springer, Dordrecht **2014**, pp. 113–128.
[2] S. Li, Y. Yan, Z. Xiong, C. W. R. Zhang, X. Wang, *J. Bioact. Compat. Polym.* **2009**, *24*, 84.
[3] C. Chimate, B. Koc, *Int. J. Adv. Manuf. Technol.* **2014**, *75*, 317.
[4] S. Sakai, H. Ohi, T. Hotta, H. Kamei, M. Taya, *Biopolymers* **2018**, *109*, e23080.
[5] N. E. Fedorovich, J. R. De Wijn, A. J. Verbout, J. Alblas, W. J. A. Dhert, *Tissue Eng., Part A* **2008**, *14*, 127.
[6] A. Faulkner-Jones, C. Fyfe, D.-J. Cornelissen, J. Gardner, J. King, A. Courtney, W. Shu, *Biofabrication* **2015**, *7*, 044102.
[7] C. Kryou, V. Leva, M. Chatzipetrou, I. Zergioti, *Bioengineering* **2019**, *6*, 95.
[8] Y. Zhao, R. Yao, L. Ouyang, H. Ding, T. Zhang, K. Zhang, S. Cheng, W. Sun, *Biofabrication* **2014**, *6*, 035001.
[9] F. P. W. Melchels, T. J. Klein, J. Malda, P. J. Bartolo, D. W. Hutmacher, *Prog. Polym. Sci.* **2012**, *37*, 1079.
[10] A. Khademhosseini, G. Camci-Unal, *3d Bioprinting in Regenerative Engineering: Principles and Applications*, CRC Press, Boca Raton, FL **2018**.
[11] R. Suntornnond, J. An, C. K. Chua, *Int. J. Bioprint.* **2017**, *3*, 83.
[12] T. Billiet, M. Vandenhaute, J. Schelfhout, S. Van Vlierberghe, P. Dubruel, *Biomaterials* **2012**, *33*, 6020.
[13] A. Dalmoro, A. A. Barba, G. Lamberti, M. Grassi, M. d'Amore, *Adv. Polym. Technol.* **2012**, *31*, 219.
[14] S. Das, F. Pati, S. Chameettachal, S. Pahwa, A. R. Ray, S. Dhara, S. Ghosh, *Biomacromolecules* **2013**, *14*, 311.
[15] T. Zhang, Y. Yan, X. Wang, Z. Xiong, F. Lin, R. Wu, R. Zhang, *J. Bioact. Compat. Polym.* **2007**, *22*, 19.

[16] P. Mozetic, S. M. Giannitelli, M. Gori, M. Trombetta, A. Rainer, *J. Biomed. Mater. Res., Part A* **2017**, *105*, 2582.
[17] V. Chiono, S. Sartori, M. Boffito, E. Gioffredi, M. Trombetta, P. Mozetic, A. Rainer, S. M. Giannitelli, WO2016194011 A1, **2016**.
[18] I. Ozbolat, M. Hospodiuk, *Biomaterials* **2016**, *76*, 321.
[19] N. E. Fedorovich, W. Schuurman, H. M. Wijnberg, H.-J. Prins, P. R. van Weeren, J. Malda, J. Alblas, W. J. A. Dhert, *Tissue Eng., Part C* **2012**, *18*, 33.
[20] E. Goulart, L. C. de Caires-Junior, K. A. Telles-Silva, B. H. S. Araujo, S. A. Rocco, M. Sforca, I. L. de Sousa, G. S. Kobayashi, C. M. Musso, A. F. Assoni, D. Oliveira, E. Caldini, S. Raia, P. I. Lelkes, M. Zatz, *Biofabrication* **2019**, *12*, 015010.
[21] A. Skardal, M. Devarasetty, C. Rodman, A. Atala, S. Soker, *Ann. Biomed. Eng.* **2015**, *43*, 2361.
[22] J. Wong, S. Shi, H. Wang, F. Xing, Y. Quan, M. Zhao, *BioRxiv* **2019**, 499723.
[23] P. Pingitore, K. Sasidharan, M. Ekstrand, S. Prill, D. Lindén, S. Romeo, *Int. J. Mol. Sci.* **2019**, *20*, 1629.
[24] N. S. Bhise, V. Manoharan, S. Massa, A. Tamayol, M. Ghaderi, M. Miscuglio, Q. Lang, Y. Shrike Zhang, S. R. Shin, G. Calzone, N. Annabi, T. D. Shupe, C. E. Bishop, A. Atala, M. R. Dokmeci, A. Khademhosseini, *Biofabrication* **2016**, *8*, 014101.
[25] X. Ma, X. Qu, W. Zhu, Y. Li, S. Yuan, H. Zhang, J. Liu, P. Wang, C. Lai, F. Zanella, G.-S. Feng, F. Sheikh, S. Chien, S. Chen, *Proc. Natl. Acad. Sci.* **2016**, *113*, 2206.
[26] D. G. Nguyen, J. Funk, J. B. Robbins, C. Crogan-Grundy, S. C. Presnell, T. Singer, A. B. Roth, *PLoS One* **2016**, *11*, e0158674.
[27] L. M. Norona, D. G. Nguyen, D. A. Gerber, S. C. Presnell, E. L. LeCluyse, *Toxicol. Sci.* **2016**, *154*, 354.
[28] X. Ma, J. Liu, W. Zhu, M. Tang, N. Lawrence, C. Yu, M. Gou, S. Chen, *Adv. Drug Delivery Rev.* **2018**, *132*, 235.
[29] A. Mazzocchi, M. Devarasetty, R. Huntwork, S. Soker, A. Skardal, *Biofabrication* **2018**, *11*, 015003.
[30] T. Hiller, J. Berg, L. Elomaa, V. Röhrs, I. Ullah, K. Schaar, A.-C. Dietrich, M. Al-Zeer, A. Kurtz, A. Hocke, S. Hippenstiel, H. Fechner, M. Weinhart, J. Kurreck, *Int. J. Mol. Sci.* **2018**, *19*, 3129.
[31] D. Choudhury, H. W. Tun, T. Wang, M. W. Naing, *Trends Biotechnol.* **2018**, *36*, 787.
[32] M. Schutte, B. Fox, M.-O. Baradez, A. Devonshire, J. Minguez, M. Bokhari, S. Przyborski, D. Marshall, *Assay Drug Dev. Technol.* **2011**, *9*, 475.
[33] S. S. Bale, L. Moore, M. Yarmush, R. Jindal, *Tissue Eng., Part B* **2016**, *22*, 383.
[34] S. M. Giannitelli, P. Mozetic, M. Trombetta, A. Rainer, in *Additive Manufacturing: Innovations, Advances, and Applications*, (Eds: T. S. Srivatsan, T. S. Sudarshan) CRC Press, Boca Raton, FL **2015**, Ch. 6.
[35] I. R. Schmolka, *J. Am. Oil Chem. Soc.* **1977**, *54*, 110.
[36] M. Müller, J. Becher, M. Schnabelrauch, M. Zenobi-Wong, *Biofabrication* **2015**, *7*, 035006.
[37] M. Kang, C. A. Day, A. K. Kenworthy, E. DiBenedetto, *Traffic* **2012**, *13*, 1589.
[38] V. Chiono, P. Mozetic, M. Boffito, S. Sartori, E. Gioffredi, A. Silvestri, A. Rainer, S. M. Giannitelli, M. Trombetta, D. Nurzynska, F. Di Meglio, C. Castaldo, R. Miraglia, S. Montagnani, G. Ciardelli, *Interface Focus* **2014**, *4*, 20130045.
[39] A. Rainer, S. M. Giannitelli, D. Accoto, S. De Porcellinis, E. Guglielmelli, M. Trombetta, *Ann. Biomed. Eng.* **2012**, *40*, 966.
[40] R. Seyedmahmoud, P. Mozetic, A. Rainer, S. M. Giannitelli, F. Basoli, M. Trombetta, E. Traversa, S. Licoccia, A. Rinaldi, *J. Biomed. Mater. Res., Part A* **2015**, *103*, 103.
[41] C. Colosi, M. Costantini, R. Latini, S. Ciccarelli, A. Stampella, A. Barbetta, M. Massimi, L. Conti Devirgiliis, M. Dentini, *J. Mater. Chem. B* **2014**, *2*, 6779.
[42] M. Esch, J. Prot, Y. Wang, P. Miller, J. Llamas-Vidales, B. A. Naughton, D. R. Applegate, M. L. Shuler, *Lab Chip* **2015**, *15*, 2269.
[43] M. Y. Zhang, P. J. Lee, P. J. Hung, T. Johnson, L. P. Lee, M. R. K. Mofrad, *Biomed. Microdevices* **2008**, *10*, 117.
[44] J. Vandesompele, K. De Preter, F. Pattyn, B. Poppe, N. Van Roy, A. De Paepe, F. Speleman, *Genome Biol.* **2002**, *3*, research0034.1.
[45] H. Weichert, I. Blechschmidt, S. Schröder, H. Ambrosius, *Allerg. Immunol.* **1991**, *37*, 139.
[46] V. Lewerenz, S. Hanelt, C. Nastevska, C. El-Bahay, E. Röhrdanz, R. Kahl, *Toxicology* **2003**, *191*, 179.
[47] H. Parikh, N. Pandita, A. Khanna, *Pharm. Biol.* **2015**, *53*, 975.
[48] S.-F. Lan, B. Starly, *Toxicol. Appl. Pharmacol.* **2011**, *256*, 62.
[49] M. R. McGill, H.-M. Yan, A. Ramachandran, G. J. Murray, D. E. Rollins, H. Jaeschke, *Hepatology* **2011**, *53*, 974.
[50] S. C. Ramaiahgari, M. W. den Braver, B. Herpers, V. Terpstra, J. N. M. Commandeur, B. van de Water, L. S. Price, *Arch. Toxicol.* **2014**, *88*, 1083.
[51] Y.-C. Toh, T. C. Lim, D. Tai, G. Xiao, D. van Noort, H. Yu, *Lab Chip* **2009**, *9*, 2026.
[52] R. Kostadinova, F. Boess, D. Applegate, L. Suter, T. Weiser, T. Singer, B. Naughton, A. Roth, *Toxicol. Appl. Pharmacol.* **2013**, *268*, 1.
[53] A. Ghallab, *EXCLI J.* **2014**, *13*, 1286.
[54] J. M. Choi, S. J. Oh, S. Y. Lee, J. H. Im, J. M. Oh, C. S. Ryu, H. C. Kwak, J.-Y. Lee, K. W. Kang, S. K. Kim, *Arch. Pharm. Res.* **2015**, *38*, 691.
[55] X. F. Koe, T. S. Tengku Muhammad, A. S.-C. Chong, H. A. Wahab, M. L. Tan, *Food Sci. Nutr.* **2014**, *2*, 500.
[56] Y. Zhengyin, G. W. Caldwell, *Curr. Top. Med. Chem.* **2001**, *1*, 403.
[57] S. Cho, A. Tripathi, G. Chlipala, S. Green, H. Lee, E. B. Chang, H. Jeong, *PLoS One* **2017**, *12*, e0182977.
[58] H. Yoshioka, T. Nonogaki, H. Ohnishi, N. Fukuishi, M. Yoshikawa, M.-Y. Gui, Y.-R. Jin, X.-W. Li, Y. Adachi, N. Ohno, K. Takeya, Y. Hitotsuyanagi, N. Miura, Y. Aoyagi, *Biomed. Res.* **2018**, *39*, 251.
[59] S. Wilkening, F. Stahl, A. Bader, R. A. Prough, *Drug Metab. Dispos.* **2003**, *31*, 1035.
[60] K. L. Schmeichel, M. J. Bissell, *J. Cell Sci.* **2003**, *116*, 2377.
[61] T. Sun, S. Jackson, J. W. Haycock, S. MacNeil, *J. Biotechnol.* **2006**, *122*, 372.
[62] V. Y. Soldatow, E. L. LeCluyse, L. G. Griffith, I. Rusyn, *Toxicol. Res.* **2013**, *2*, 23.
[63] T. Grix, A. Ruppelt, A. Thomas, A.-K. Amler, B. Noichl, R. Lauster, L. Kloke, *Genes* **2018**, *9*, 176.
[64] A. Asthana, W. S. Kisaalita, *Drug Discovery Today* **2012**, *17*, 810.
[65] F. Hirschhaeuser, H. Menne, C. Dittfeld, J. West, W. Mueller-Klieser, L. A. Kunz-Schughart, *J. Biotechnol.* **2010**, *148*, 3.
[66] A. M. Larson, J. Polson, R. J. Fontana, T. J. Davern, E. Lalani, L. S. Hynan, J. S. Reisch, F. V. Schiødt, G. Ostapowicz, A. O. Shakil, W. M. Lee, *Hepatology* **2005**, *42*, 1364.
[67] J. G. M. Bessems, N. P. E. Vermeulen, *Crit. Rev. Toxicol.* **2001**, *31*, 55.
[68] H. Jaeschke, M. L. Bajt, *Toxicol. Sci.* **2006**, *89*, 31.
[69] S. R. Khetani, S. N. Bhatia, *Nat. Biotechnol.* **2008**, *26*, 120.
[70] E. L. LeCluyse, R. P. Witek, M. E. Andersen, M. J. Powers, *Crit. Rev. Toxicol.* **2012**, *42*, 501.
[71] S. A. Langhans, *Front. Pharmacol.* **2018**, *9*, 6.
[72] S. R. Caliari, J. A. Burdick, *Nat. Methods* **2016**, *13*, 405.
[73] Y. S. Zinchenko, L. W. Schrum, M. Clemens, R. N. Coger, *Tissue Eng.* **2006**, *12*, 751.
[74] V. L. Tsang, A. A. Chen, L. M. Cho, K. D. Jadin, R. L. Sah, S. DeLong, J. L. West, S. N. Bhatia, *FASEB J.* **2007**, *21*, 790.
[75] M. Yamada, A. Hori, S. Sugaya, Y. Yajima, R. Utoh, M. Yamato, M. Seki, *Lab Chip* **2015**, *15*, 3941.
[76] M. Gori, B. Barbaro, M. Arciello, R. Maggio, C. Viscomi, A. Longo, C. Balsano, *J. Cell. Physiol.* **2014**, *229*, 1182.
[77] N. B. Javitt, *FASEB J.* **1990**, *4*, 161.
[78] K. Bhadriraju, C. S. Chen, *Drug Discovery Today* **2002**, *7*, 612.